JOURNAL OF AIRCRAFT
Vol. 45, No. 3, May–June 2008

Reynolds-Averaged Navier–Stokes Simulation of Low-Reynolds-Number Airfoil Aerodynamics

Lei Tang*
ZONA Technology, Inc., Scottsdale, Arizona 85258

DOI: 10.2514/1.21995

A simple procedure has been developed to improve Reynolds-averaged Navier–Stokes simulation of low-Reynolds-number airfoil aerodynamics, especially the laminar separation bubble. First, a laminar Navier–Stokes computation is performed for the selected low-Reynolds-number SD7003 airfoil case. The importance of sufficient grid resolution in the normal direction and numerical iteration has been emphasized for achieving a relatively stable, time-averaged, two-dimensional, laminar separation solution. Based on this laminar solution, the separation-induced transition is determined as the point at which the tangential velocity adjacent to the solid surface reverses its direction for the second time after the laminar separation. Then a Reynolds-averaged Navier–Stokes computation is further performed with zero production terms in the selected turbulence model before the transition point and with the complete turbulence model after the transition point. As a result, similar to large-eddy simulation and direct numerical simulation, a Reynolds-averaged Navier–Stokes approach using the Spalart–Allmaras model is able to capture a laminar separation bubble without any external transition mechanism. The robustness of the approach is validated with several other low-Reynolds-number airfoil cases.

I. Introduction

RECENTLY, growing interest in micro air vehicles has renewed extensive studies on low-Reynolds-number airfoil aerodynamics [1,2]. Different from our familiar high-Reynolds-number aerodynamics, low-Reynolds-number airfoil aerodynamics is characterized with the existence of a laminar separation bubble on the upper surface of the airfoil, which involves laminar boundary-layer separation, separation-induced transition, and turbulent reattachment. To accurately predict low-Reynolds-number airfoil aerodynamics, a computational tool should have the capability of predicting the laminar separation bubble.

Various computational approaches have been explored for prediction of low-Reynolds-number aerodynamics, ranging from viscous/inviscid interactive methods [3–6] through Reynolds-averaged Navier–Stokes (RANS) [7–11] and unsteady RANS (URANS) [2] methods to large-eddy simulation (LES) and direct numerical simulation (DNS) [2,12] methods. Except for RANS using low-Reynolds-number versions of the turbulence models [7–10] and LES/DNS [2,12] in which the separation-induced transition occurs naturally, all other approaches require an external mechanism to find the transition position. The most popular method used in practice is still the semi-empirical e^N method [13,14] and its various approximations. For instance, Shum and Marsden [3] used Van Ingen's shortcut e^N method for fast determination of the transition location. Drela and Giles [4] came out with a more sophisticated approximation, the so-called envelop method, and Dini et al. [5,6] adopted the table lookup approach. Stock and Haase [11] and Yuan et al. [2] further combined, respectively, RANS and URANS with the e^N method. The importance of sufficient grid resolution inside the boundary layer was emphasized in [11] for the accuracy of stability analysis based on the Navier–Stokes laminar solutions. On the other hand, although there is no need for an external transition mechanism, the LES/DNS approach is computationally too intensive for engineering applications, and the robustness of using a low-Reynolds-number version of the turbulence model for transition prediction is questionable. Whereas Wilcox [9] presented some promising results for the flat-plate case, the same low-Reynolds-number version of Wilcox's k–ω model is found to predict the transition location too early in [10]. Furthermore, the transitional result given by a low-Reynolds-number version of the turbulence model is also found to be initial-condition-dependent [8].

In this paper, a systematic RANS simulation will be performed first for the low-Reynolds-number SD7003 airfoil case presented in [1]. A brief description of the employed numerical algorithm is given in Sec. II. This is followed by the presentation and discussion of the laminar solution in Sec. III. Then Sec. IV presents a simple method for determination of the transition point from the laminar solution, and some RANS simulation results are further presented in Sec. V. Finally, Sec. VI presents the application of the approach to several other low-Reynolds-number airfoil cases, for validation.

II. Numerical Algorithm

The computational fluid dynamics (CFD) code used in this study is CFL3D v6 [15], which is developed and supported by NASA Langley Research Center. This is a three-dimensional, thin-layer, Reynolds-averaged Navier–Stokes solver using an implicit, approximately factored, finite volume, upwind, and multigrid algorithm. It employs formally third-order, upwind-biased, spatial differencing for the inviscid terms, with flux limiting in the presence of shocks. Both flux-difference and flux-vector splitting methods are available in the code. The flux-difference splitting method of Roe [16] is employed in the present computations for accurate viscous computations. On the other hand, the viscous terms are discretized with second-order central differencing.

There are numerous turbulence models available in the CFL3D code. According to URANS results presented in [2], Menter's two-layer baseline (BSL) model [17] and Launder-Sharma's low-Reynolds number version of k–ε model [7] give the most accurate prediction of Reynolds-stress distribution for the investigated low-Reynolds-number SD7003 airfoil case. So we have implemented Menter's two-layer BSL model [17] and the Jones–Launder k–ε model [18] in the CFL3D code and compare them with the existing Spalart–Allmaras model [19] and Abid's low-Reynolds-number version of the k–ε model [8] in the code.

Because CFL3D is a compressible CFD code, the Weiss–Smith low-Mach-number preconditioning technique [20] is used in the

Presented as Paper 0249 at the 44th Aerospace Sciences Meeting and Exhibit, Reno, NV, 9–12 January 2006; received 22 December 2005; revision received 22 April 2006; accepted for publication 22 April 2006.

*Computational Fluid Dynamics Manager; currently, President, D&P LLC, Phoenix, AZ 85018. Associate Fellow AIAA.

code to improve the convergence performance of incompressible flow simulation.

III. Laminar Solution of the Low-Reynolds-Number SD7003 Airfoil Case

The low-Reynolds-number SD7003 airfoil case in [1] is selected for a systematic RANS study, because a stable long separation bubble is found over the upper surface of the airfoil in the tests. The Technical University of Braunschweig (TUBS) wind-tunnel test conditions are adopted as the flow conditions for computations. According to [1], the freestream Reynolds number is 60,000, based on the airfoil chord length, and the angle of attack is 4 deg. We estimate the Mach number to be 0.013 and the freestream turbulence level is chosen as 0.08%.

A C-type grid is used in the computations. As shown in Fig. 1, there are 386 points along the wraparound direction, with 280 points on the airfoil surface and 151 points in the normal direction, with the first grid spacing from the surface as 10^{-6} of the chord length. The outer boundaries of the grid are extended to 20 chords in all directions.

A laminar computation is performed first. The predicted surface C_p distributions over the upper surface of the airfoil after 5000, 10,000, 15,000, 20,000, 25,000, 30,000, and 35,000 iterations are presented in Fig. 2. It is found that after 10,000 iterations, the obtained surface C_p distribution is still like the C_p distribution without the bubble perturbation. By that time, as shown in the convergence history presented in Fig. 3, the numerical residual has already dropped by three orders of magnitude. Therefore, many

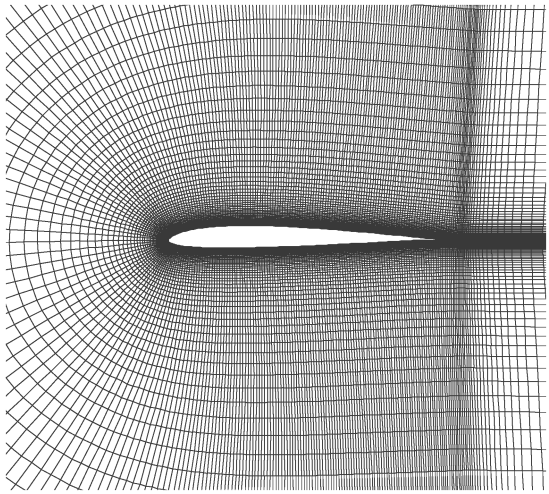

Fig. 1 Computational grid.

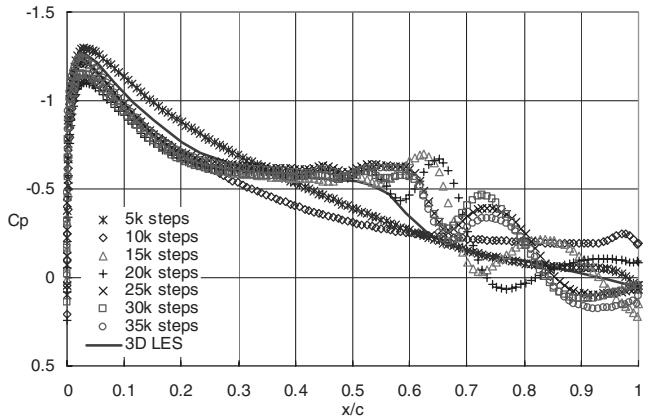

Fig. 2 Predicted surface C_p distributions on the upper surface of the SD7003 airfoil.

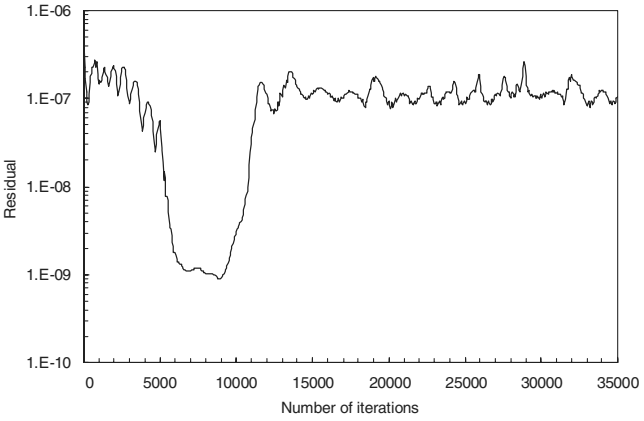

Fig. 3 Convergence history.

people may stop the computation there, thinking that a fully converged solution is obtained and that without any external transition mechanism, the existing CFD approach is not able to capture the laminar separation bubble. However, if one is not fooled by the misleading convergence history and keeps running the computation after 15,000 iterations, as shown in Fig. 2, a surface C_p distribution with the bubble perturbation starts to be captured in the computations, with a C_p plateau between the separation and transition. After 25,000 iterations, the predicted surface C_p distribution becomes quite stable. This is different from the findings by Pauley et al. [21], in which a two-dimensional laminar separation solution is found to be quite unstable.

Also shown in Fig. 2 is the 3D LES result from [2]. It is found that our converged laminar solution agrees with the LES solution relatively well up to the transition point. After the transition point, there is a much larger discrepancy between the two solutions. Most notably, different from the LES result, our converged laminar solution has several artificial humps in the surface C_p distribution after the transition point. Looking from a DNS point of view, this indicates that our employed numerical method and mesh are able to resolve the simulated laminar flow quite well but are still unable to resolve the turbulent flow yet. A proper turbulence model is required for simulation of the flow after the transition point.

It is noteworthy that after 9000 iterations, as shown in Fig. 3, the numerical residual quickly jumps by two orders of magnitude and oscillates around that level. As will be shown later, this is solely because we do not turn on a turbulence model from the transition point in the computation. Based on the surface C_p distribution shown in Fig. 2 and the velocity fields shown in Fig. 4, the big jump of numerical residual after 9000 iterations indicates the transition of the numerical solution from one without the bubble perturbation to one with the bubble perturbation.

Figure 4 further presents the predicted velocity fields, including some streamlines, after 5000, 10,000, 15,000, 20,000, 25,000, 30,000, and 35,000 iterations and compares with U.S. Air Force Research Laboratory (AFRL) test data in [1]. It is found that the flowfield solution obtained after 5000 iterations has no separation at all. By 10,000 iterations, the trailing-edge separation is captured, and by 15,000 iterations, the laminar separation bubble further starts to be captured. After 25,000 iterations, the predicted flow patterns are quite stable. All these observations are consistent with the surface C_p surface distributions shown in Fig. 2. Compared with AFRL test data, the converged laminar solution of the separation bubble is much longer and thicker, because there are three vortical structures inside the separation bubble instead of one, as found in the test. This also explains those artificial humps found in the converged surface C_p distribution shown in Fig. 2. Apparently, the latter two vortical structures are due to the lack of transition to turbulence in the computation and they are not physical.

In addition to insufficient iterations, another possible reason for people to miss capturing a stable laminar separation bubble in computation is the insufficient grid resolution. For a typical viscous

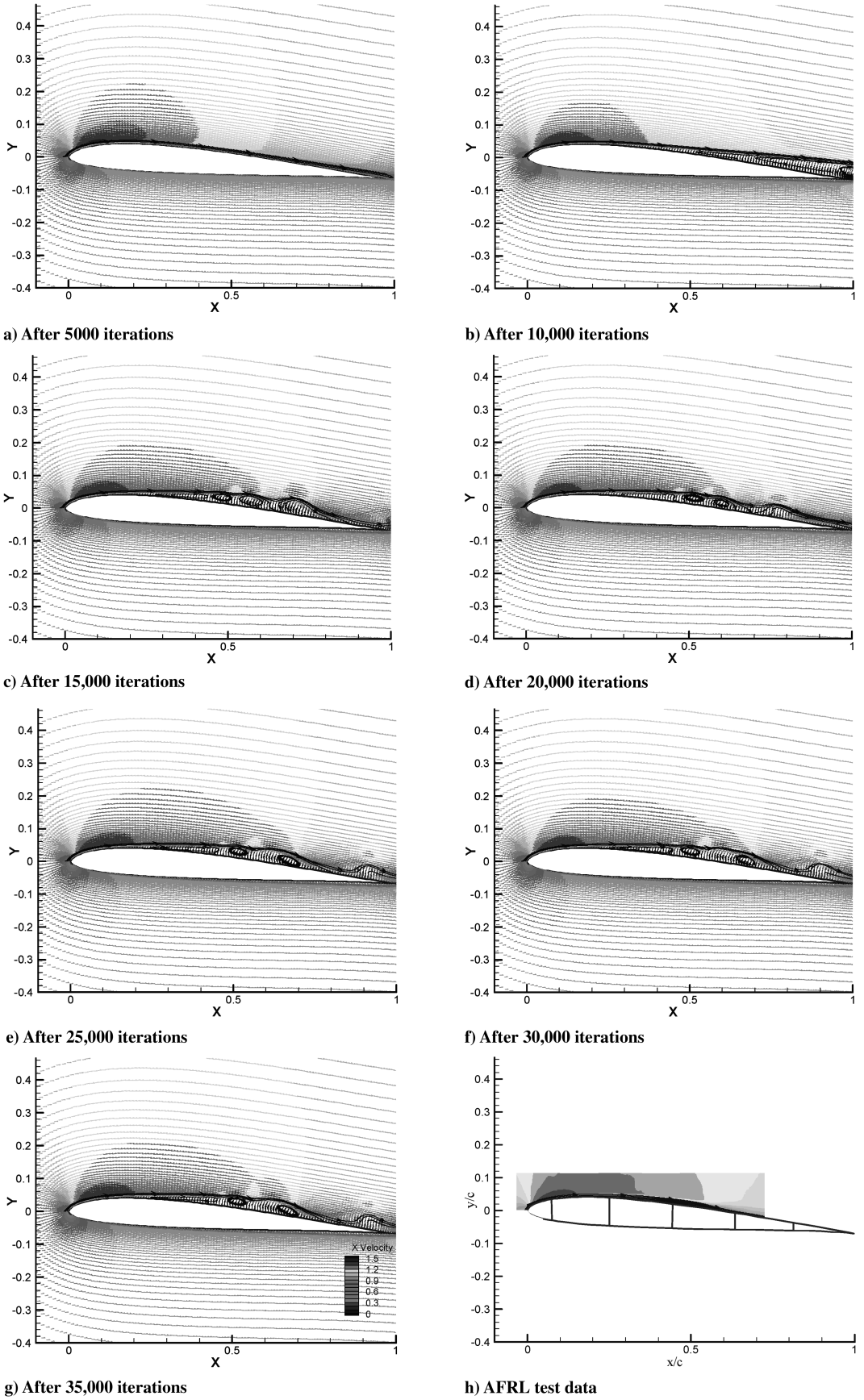

Fig. 4 Velocity field and streamlines.

computation such as the current one, a mesh with 91 points in the normal direction and the first grid spacing of 10^{-5} of the chord length from the surface is usually sufficient to resolve the boundary-layer flows. However, as shown in Fig. 5, the surface C_p distribution predicted on this coarser mesh is very unstable (the same as the findings by Pauley et al. [21]). Apparently, although the resolution of this grid is sufficient to resolve the boundary layer, it is still not sufficient to resolve the laminar flow separation. Note that for

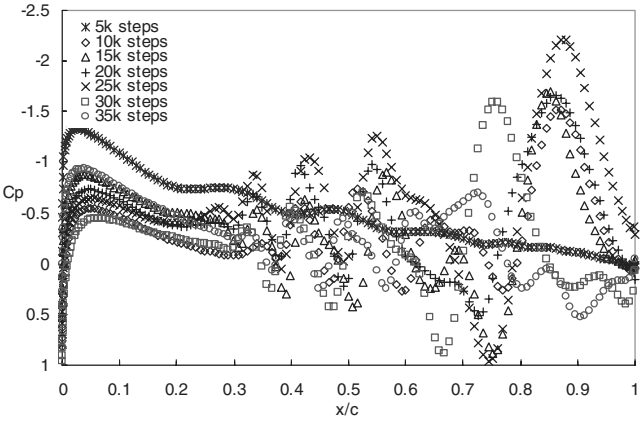

Fig. 5 Predicted surface C_p distributions on a coarser mesh with 91 points in the normal direction.

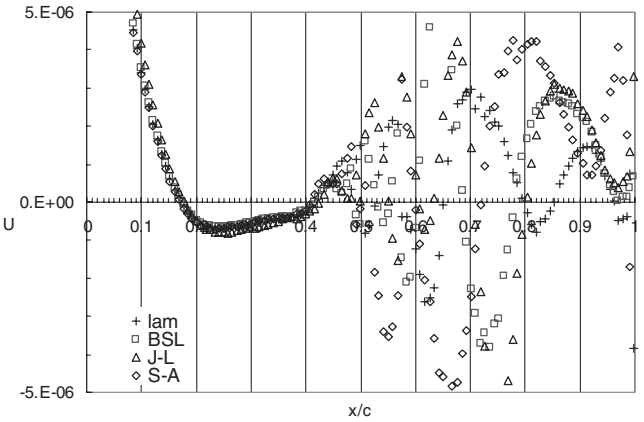

Fig. 7 Distribution of nondimensional tangential velocity next to the upper surface of the SD7003 airfoil.

simulation of laminar separation, the grid resolution requirement should be the same for RANS and DNS.

IV. Specification of the Transition Point

A key for prediction of the laminar separation bubble is to accurately locate the position of separation-induced transition. The existing transition-prediction methods range from simple empirical correlations through semi-empirical methods such as the e^N method to direct numerical simulations. The e^N method, based on linear stability analysis and the empirical input of N at transition, is the most popular in practice. Stock and Haase [11] investigated the feasibility of coupling the e^N method to RANS computation. It is found that to produce reliable laminar data for the stability analysis, a sufficiently large and constant number of grid points are required inside the viscous layer. This requirement, combined with the stability analysis, render the resulting RANS computation much more intensive. In the following, we will present a much simpler method to locate the transition position.

Figure 6 is an enlargement of Fig. 4g near the upper surface of the airfoil, in which the flow next to the solid surface is shown to reverse the direction around $0.18c$, indicating the separation of laminar flow. From the separation point, a dividing line forms. Above this line, the flow moves downstream, and below this line, the flow moves upstream, resulting in a strong free shear layer there. This shear layer starts to become unstable from $0.4c$ and eventually rolls up into a vortex. At the same time, the reversed flow next to the upper surface reverses the direction again and moves downstream, whereas, in reality, this should happen until the reattachment. Both phenomena are not physical and can be used as indications of the fact that a laminar solution is unsustainable from there and that the transition to turbulence should take place.

To give a quantitative definition of the separation-induced transition position, the distribution of the nondimensional tangential velocity (i.e., Mach number) at the grid points next to the upper surface of the SD7003 airfoil is further presented in Fig. 7. It is found that the laminar solution is very smooth before the second flow reverse, but becomes quite unstable after that. This further supports the preceding finding that the transition to turbulence should take place where the laminar solution next to the solid surface reverses the direction for the second time after the laminar separation. According to Fig. 7, the transition point for this low-Reynolds-number SD7003 airfoil case is at $0.416c$, whereas the laminar separation point is at $0.176c$.

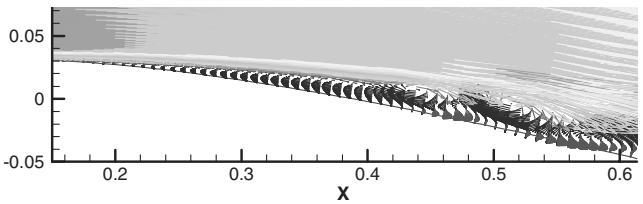

Fig. 6 Velocity fields adjacent to the upper surface of the SD7003 airfoil.

Also included in Fig. 7 are the laminar solutions from RANS simulations with zero production terms in the selected turbulence models. The use of such RANS solutions as the laminar solutions has two advantages. First, this will introduce less perturbation to the subsequent RANS computations, in which the production terms in the turbulence models are turned on after the transition point. Second, but more important, the effect of the freestream turbulence level on the transition point can be taken into account through the boundary conditions. It is found that the two solutions given by the laminar computation and the RANS simulation with the Spalart–Allmaras one-equation model (S–A) [19] are almost indistinguishable up to the transition point. On the other hand, the solution given by the RANS simulation with the Jones–Launder k–ε model (J–L) [18] deviates the most from the laminar solution. The transition point given by the RANS simulation with Menter's two-layer BSL model [17] is one grid point later than the laminar solution and the S–A solution, whereas the J–L model delays the predicted transition position by another grid point from the BSL solution. All these findings are further supported by the surface C_p distributions shown in Fig. 8. Among all RANS solutions, the S–A solutions are the closet to the laminar solutions in Fig. 2. On the other hand, the initial discrepancy between the RANS solutions given by the two-equation models and the laminar solutions is quite large. However, the differences between the solutions up to the transition point become smaller with iterations. From the transition point, moreover, the solutions given by RANS with the two-equation models are found less stable than the laminar solutions.

V. RANS Solution of the Low-Reynolds-Number SD7003 Airfoil Case

After locating the transition point, RANS simulations are performed with zero production terms in the selected turbulence model before the transition point and with the complete turbulence model after the transition point. To compare the convergence performance with the preceding laminar computation, we start RANS computation from the uniform freestream conditions again, rather than restart the computation from the preceding RANS solutions with zero production terms in the selected turbulence model. It is found in Fig. 9 that the numerical residual of RANS simulation with the S–A model is initially almost the same as the laminar solution. However, different from the laminar solution, the numerical residual of RANS simulation does not jump back after 9000 iterations. Instead, the numerical residual drops monotonically, due to the nonzero production terms in the S–A model after the transition point.

Figure 10 presents the predicted surface C_p distributions over the upper surface of the airfoil by RANS simulations with different

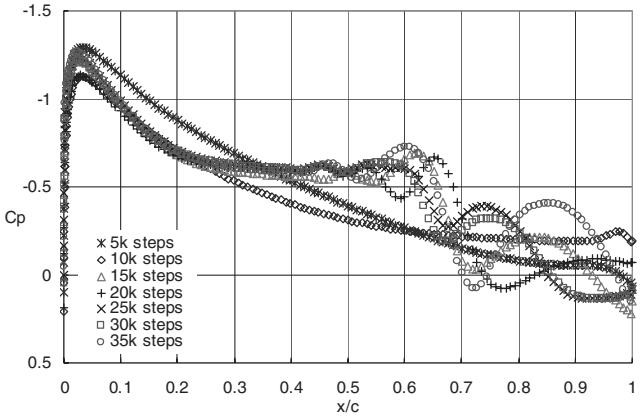

a) Spalart-Allmaras model

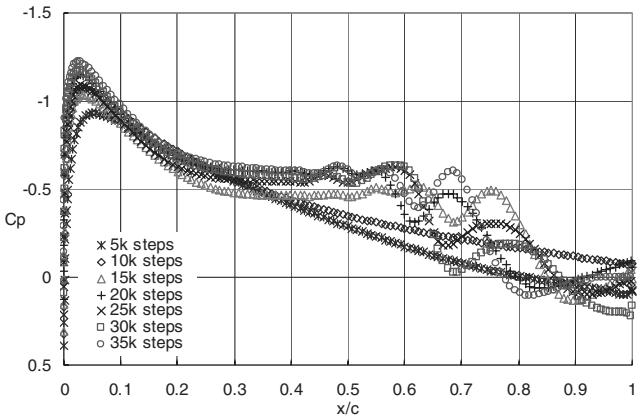

b) Menter two-layer BSL model

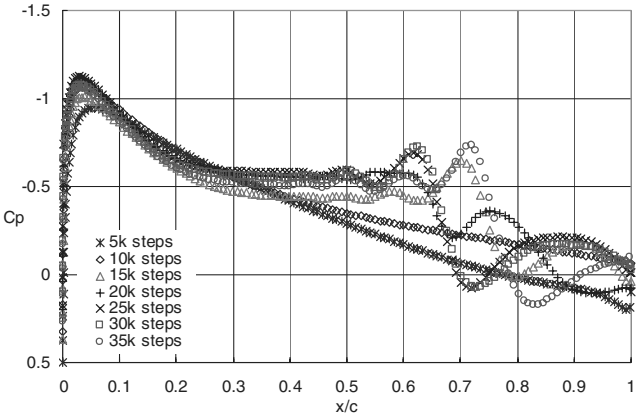

c) Jones-Launder k–ε model

Fig. 8 Surface C_p distributions predicted by RANS with zero production terms.

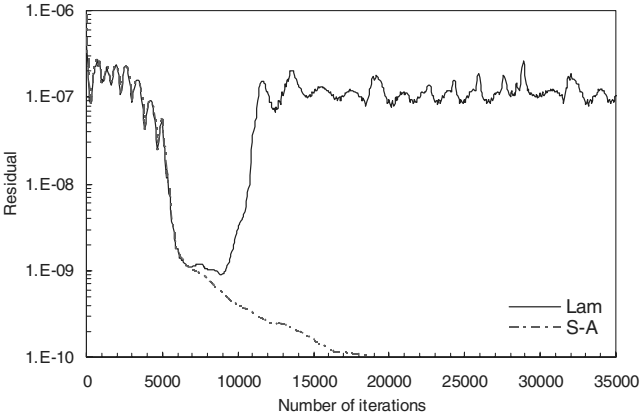

Fig. 9 Convergence history.

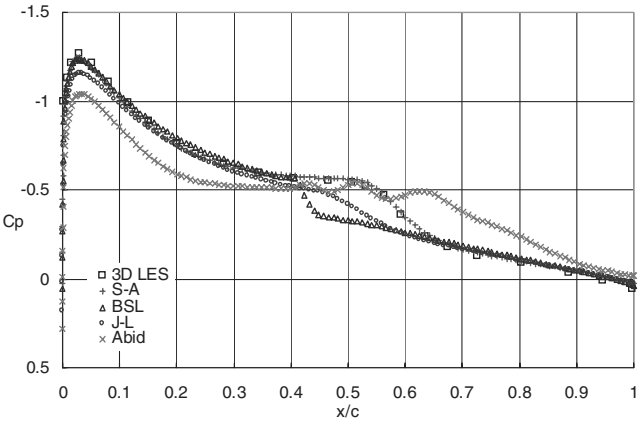

Fig. 10 Surface C_p distributions predicted by RANS with the transition mechanism.

turbulence models, along with the 3D LES result in [2]. It is found that the converged S–A solution is almost indistinguishable from the 3D LES result. On the other hand, the solutions given by the two-equation models are quite different from the 3D LES result. It is interesting to note that, different from Horton's bubble model, the S–A solution does not immediately accelerate the deceleration process after the transition point. Instead, the predicted flow keeps the same deceleration rate for a while and starts to decelerate quickly until after $0.532c$. On the other hand, consistent with Horton's model, the converged BSL solution speeds up the deceleration immediately after the transition point. The predicted deceleration rate is also larger than the 3D LES result, indicating the possibility of overpredicting Reynolds stress there. Furthermore, the converged J–L solution is found between the preceding two RANS solutions. The deceleration after the transition point picks up before the S–A solution but after the BSL solution. The predicted deceleration rate is smaller than those given by the other approaches, indicating the possibility of underpredicting Reynolds stress there. Also included in Fig. 10 is the result given by RANS simulation with Abid's low-Reynolds-number version of the k–ε model [8], without specification of the transition point. It is found that this low-Reynolds-number version of the k–ε model does capture the laminar separation bubble automatically, but is unable to completely remove those humps found in the preceding laminar C_p distribution associated with the artificial vortical structures inside the boundary layer. Therefore, the flow reattaches to the surface much later than the 3D LES result, and the separation bubble is unreasonably long and thick.

The predicted Reynolds-stress distributions by RANS with the first three turbulence models are presented in Fig. 11, in comparison with AFRL test data in [1]. It is surprising to see that all RANS computations, especially Menter's two-layer BSL model [17], underpredict the maximum absolute value of Reynolds stress. This is inconsistent with the predicted surface C_p distributions shown in Fig. 10. A possible reason for the inconsistency is that is we compare our RANS results with AFRL water-tunnel test data instead of TU-BS wind-tunnel test data. According to [2], the maximum absolute value of the Reynolds stress of AFRL water-tunnel test data is slightly higher than TU-BS wind-tunnel test data. On the other hand, the starting position and shape of the predicted Reynolds-stress pocket by S–A and J–L models agree with the test data, whereas the Reynolds-stress pocket given by the BSL model starts too early, especially the predicted Reynolds stress by the BSL model, which jumps to its maximum absolute value too quickly after the transition point. This explains why the BSL surface C_p solution has a turning point immediately after the transition. Consistent with the surface C_p distributions shown in Fig. 10, the BSL model produces the largest

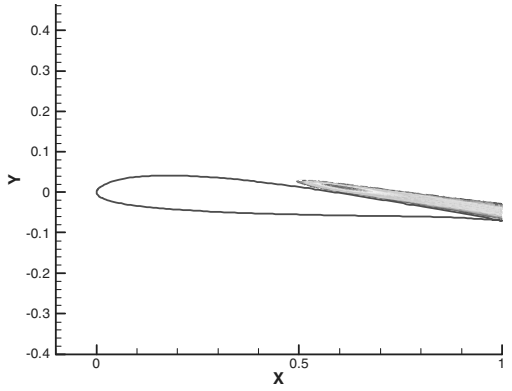

a) S-A model

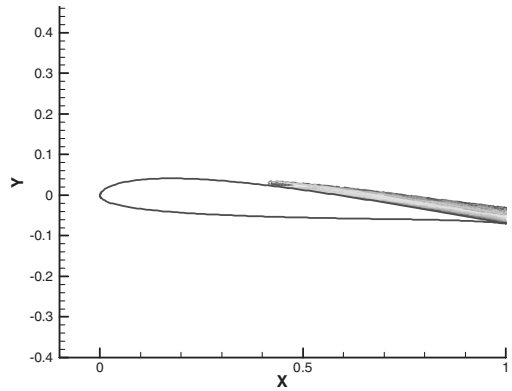

b) Two-layer BSL model

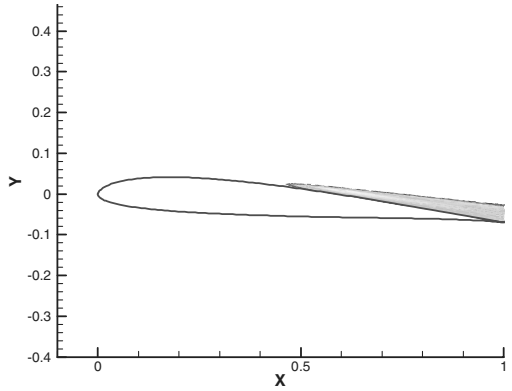

c) J-L model

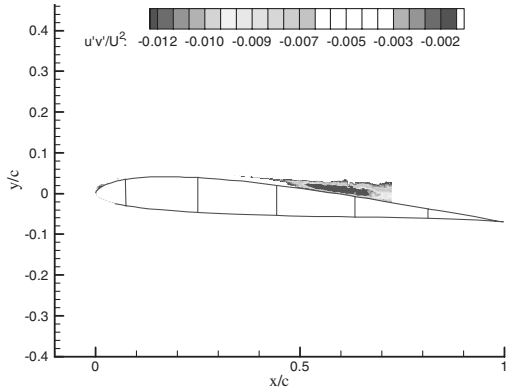

d) AFRL test data

Fig. 11 Reynolds-stress distributions.

maximum absolute value of Reynolds stress among all RANS solutions, whereas the J–L model gives the smallest value.

To further compare the predicted laminar separation bubble with AFRL test data, Fig. 12 presents the velocity contours and

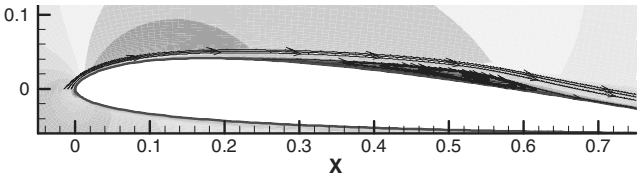

a) S-A model

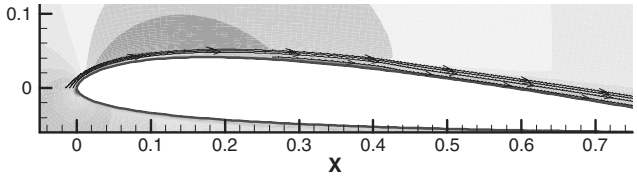

b) Two-layer BSL model

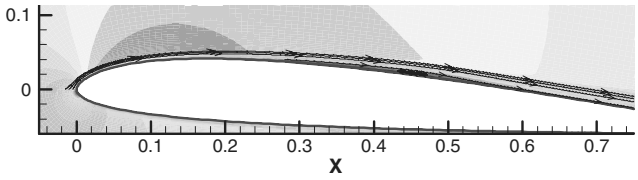

c) J-L model

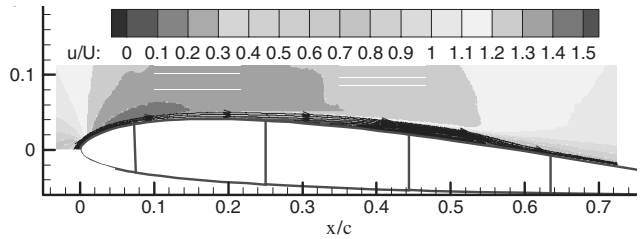

d) AFRL test data

Fig. 12 Velocity contours and streamlines.

streamlines around the SD7003 airfoil. It is found that the separation bubble predicted by the S–A model is the closest to the test data, including both the length and thickness, whereas those given by the two-equation models are too short and too thin, especially the separation bubble from the BSL model, which is almost negligible.

These facts can be more clearly seen in the distributions of tangential velocity next to the upper surface of the airfoil shown in Fig. 13. It is found that after turning on the production terms in the selected turbulence model after the transition point, the laminar separation point can be modified to a significantly later position,

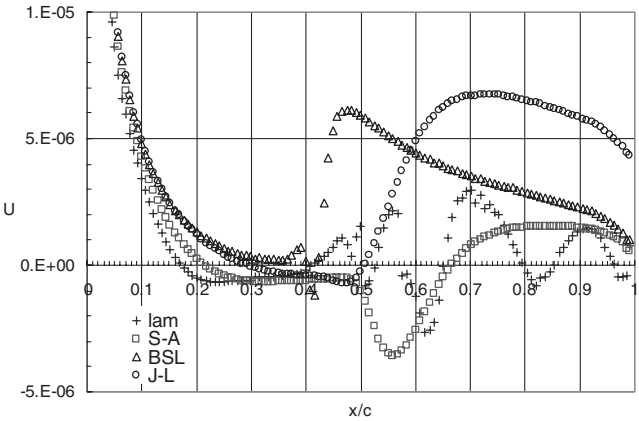

Fig. 13 Tangential velocity distribution next to the upper surface of the SD7003 airfoil.

Table 1 Comparison of numerical and experimental results

	x_s/c	x_t/c	x_r/c
Test (TUBS)	0.30	0.55	0.62
Test (AFRL)	0.18	0.47	0.58
3D LES	0.25	0.49	0.60
S–A	0.22	0.42	0.67
BSL	0.40	0.42	0.42
J–L	0.30	0.43	0.51

especially for the BSL solution, in which there are only two grid points in the reversed flow state, due to overprediction of Reynolds stress.

Table 1 presents a quantitative comparison between the numerical separation bubble and the existing test data in [1]. Compared with the test data and 3D LES result, the S–A model is found to predict a longer bubble, whereas the two-equation models give a shorter bubble. Again, the separation bubble predicted by the two-layer BSL model is almost negligible.

VI. Application to Other Low-Reynolds-Number Airfoil Cases

To examine the robustness of the preceding method for prediction of low-Reynolds-number airfoil aerodynamics, we will further investigate several other low-Reynolds-number airfoil cases. This time, RANS computations with a zero production term in the selected S–A model are performed first to provide the baseline laminar solution. After determination of the transition point, RANS computations with the complete S–A model after the transition point are restarted from the preceding RANS laminar solutions instead of the uniform freestream conditions, for less numerical iterations before a fully converged RANS solution is achieved.

The first low-Reynolds-number airfoil case investigated is the Eppler387 airfoil case in [22]. It is noteworthy that the test model has a blunted trailing edge, with the thickness of 0.167% of the chord length. Our numerical results indicate whether or not modeling this blunt trailing edge has a large impact on the predicted C_p suction peak value, especially for higher angles of attack. Figure 14 presents the two types of meshes used in computation. Figure 14a is a C-mesh with a sharp trailing edge. There are 301 points in the wraparound direction, 201 points on the body, and 151 points in the normal direction, with the first grid spacing from the surface as 10^{-6} of the chord length. Figure 14b is an O-mesh with a blunted trailing edge. There are 251 points in the wraparound direction, 11 points to cover the blunted trailing edge, and 111 points in the normal direction, with the first grid spacing from the surface as 10^{-6} of the chord length. The outer boundary of the meshes is extended to 20 chords in all directions.

Figure 15 presents the predicted surface C_p distributions on the two computational grids for the case with the freestream Mach number of 0.08, Reynolds number of 100,000, and angle of attack of 7 deg, in comparison with the test data from [22]. It is found that without modeling the blunt trailing edge, the predicted peak value of the surface C_p suction on the C-mesh is much lower than the test data. On the other hand, with modeling the blunt trailing edge, the predicted surface C_p distribution on the O-mesh is in good agreement with the test data.

The second case investigated is the low-Reynolds-number LA203A airfoil case in [23]. An O-mesh is used for this case. As shown in Fig. 16, there are 161 points in the wraparound direction and 121 points in the normal direction, with the first grid spacing from the surface as 10^{-6} of the chord length. The outer boundary of the grid is extended to 20 chords in all directions.

In this case, the freestream Mach number is 0.1, the Reynolds number is 250,000, and the angle of attack is 4 deg. Based on the baseline laminar solution, the transition point is found at $0.574c$. The predicted surface C_p distribution is presented in Fig. 17 in comparison with the test data in [23]. A good agreement is found.

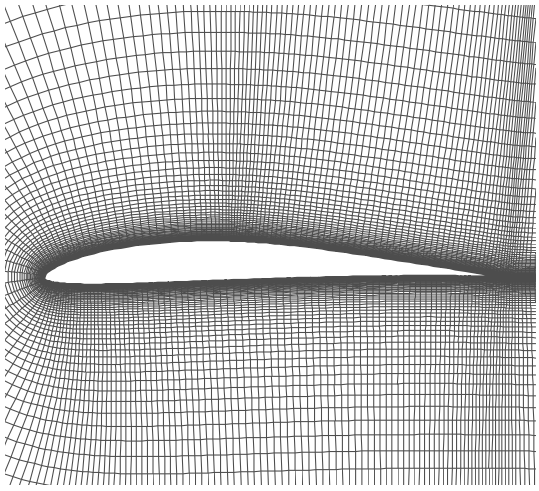

a) C-mesh with sharp trailing edge

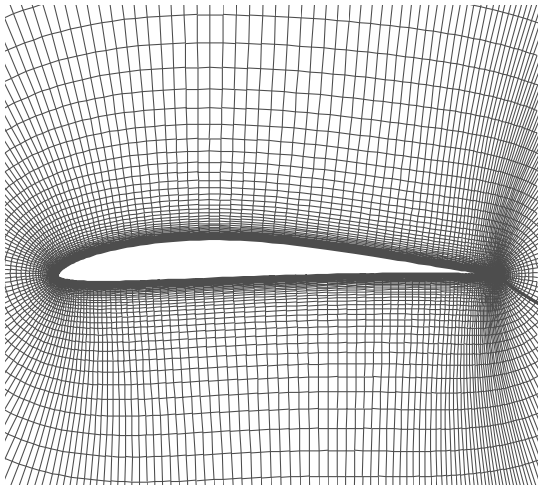

b) O-mesh with blunt trailing edge

Fig. 14 Computational grids used for the Eppler387 airfoil case.

The last case considered is the low-Reynolds-number LNV109A airfoil case in [23]. A C-mesh is used for this case. As shown in Fig. 18, there are 281 points in the wraparound direction with 181 points on the body and 121 points in the normal direction with the first grid spacing from the surface as 10^{-6} of the chord length. The outer boundary of the grid is extended to 20 chords in all directions.

Figure 19 presents the predicted surface C_p distribution in comparison with the test data in [23] for the case with the freestream Mach number of 0.1, Reynolds number of 375,000, and angle of

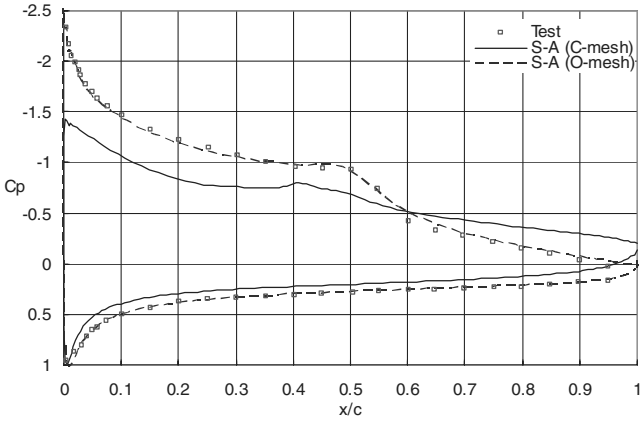

Fig. 15 Surface C_p distribution for the Eppler387 airfoil case.

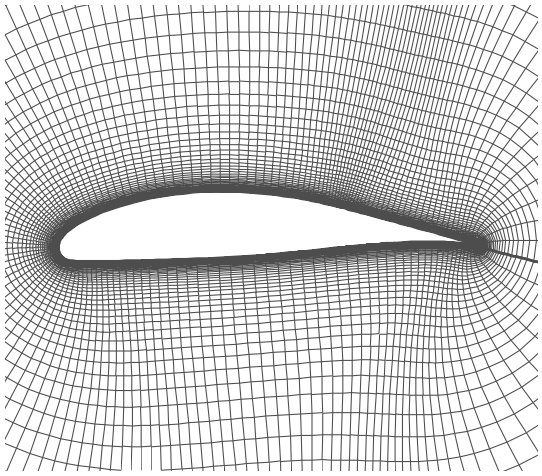

Fig. 16 Computational grid used for the LA203A airfoil case.

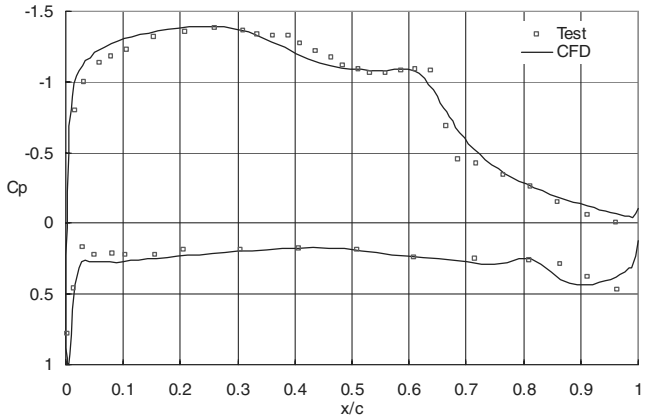

Fig. 17 Surface C_p distribution for the LA203A airfoil case.

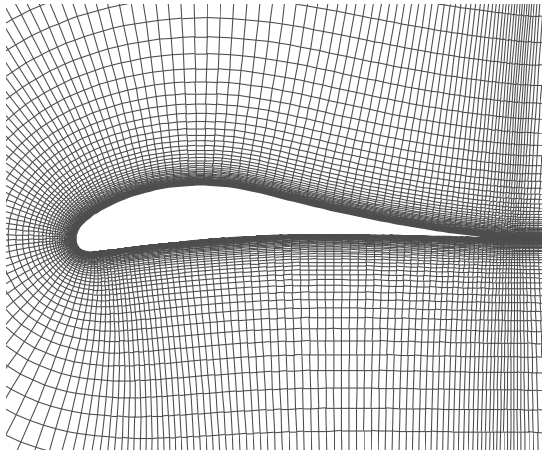

Fig. 18 Computational grid used for the LNV109A airfoil case.

attack of 8 deg. This time the transition point is found at $0.365c$. Again, the predicted surface C_p distribution is found in good agreement with the test data.

VII. Conclusions

Obtaining a good baseline laminar solution is crucial to achieve an accurate prediction of low-Reynolds-number airfoil aerodynamics. The importance of sufficient grid resolution and numerical iterations was emphasized for obtaining such a solution. The position of the separation-induced transition can be determined as the point at which the tangential velocity adjacent to the solid surface reverses its direction for the second time after the laminar separation. After determination of the transition point, the laminar separation bubble can be accurately simulated with the RANS approach using the Spalart–Allmaras model with zero and complete production terms before and after the transition point, respectively. The approach is much simpler and more efficient than coupling the e^N method to the RANS, LES, and DNS approaches.

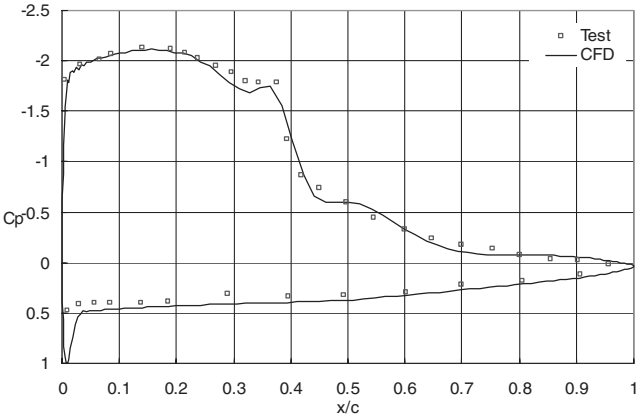

Fig. 19 Surface C_p distribution for the LNV109A airfoil case.

Acknowledgments

This work is sponsored by U.S. Air Force Research Laboratory (AFRL), Small Business Innovation Research Phase I contract FA8650-05-M-3548. The technical monitor is Trenton White. The author gratefully acknowledges Michael V. Ol of the AFRL for providing us his test data and Weixing Yuan of the National Research Council of Canada for technical discussion.

References

[1] Ol, M. V., McAuliffe, B. R., Hanff, E. S., Scholz, U., and Kähler, C., "Comparison of Laminar Separation Bubble Measurements on a Low Reynolds Number Airfoil in Three Facilities," AIAA Paper 2005-5149, 2005.

[2] Yuan, W. X., Khalid, M., Windte, J., Scholz, U., and Radespiel, R., "An Investigation of Low-Reynolds-Number Flows Past Airfoils," AIAA Paper 2005-4607, 2005.

[3] Shum, Y. K., and Marsden, D. J., "Separation Bubble Model for Low Reynolds Number Airfoil Applications," *Journal of Aircraft*, Vol. 31, No. 4, 1994, pp. 761–766.

[4] Drela, M., and Giles, M. B., "Viscous-Inviscid Analysis of Transonic and Low Reynolds Number Airfoils," *AIAA Journal*, Vol. 25, No. 10, 1987, pp. 1347–1355.

[5] Dini, P., Selig, M. S., and Maughmer, M. D., "Simplified Linear Stability Transition Prediction Method for Separated Boundary Layers," *AIAA Journal*, Vol. 30, No. 8, 1992, pp. 1953–1961.

[6] Dini, P., and Maughmer, M. D., "Locally Interactive Laminar Separation Bubble Model," *Journal of Aircraft*, Vol. 31, No. 5, 1994, pp. 802–810.

[7] Launder, B. E., and Sharma, B. I., "Application of the Energy-Dissipation Model of Turbulence to the Calculation of Flow Near a Spinning Disc," *Letters in Heat and Mass Transfer*, Vol. 1, Nov.–Dec. 1974, pp. 131–138. doi:10.1016/0094-4548(74)90150-7

[8] Abid, R., "Evaluation of Two-Equation Turbulence Models for Predicting Transitional Flows," *International Journal of Engineering Science*, Vol. 31, No. 6, 1993, pp. 831–840. doi:10.1016/0020-7225(93)90096-D

[9] Wilcox, D. C., "Simulation of Transition with a Two-Equation Turbulence Model," *AIAA Journal*, Vol. 32, No. 2, 1994, pp. 247–255.

[10] Liu, S. Z., and Tsai, H. M., "Simulation of Boundary Layer Transition with a Modified k–ω Model," AIAA Paper 98-0340, 1998.

[11] Stock, H. W., and Haase, W., "Feasibility Study of e^N Transition Prediction in Navier–Stokes Methods for Airfoils," *AIAA Journal*, Vol. 37, No. 10, 1999, pp. 1187–1196.

[12] Spalart, P. R., and Strelets, M. Kh., "Mechanism of Transition and Heat Transfer in a Separation Bubble," *Journal of Fluid Mechanics*, Vol. 403, 2000, pp. 329–349.
doi:10.1017/S0022112099007077

[13] Van Ingen, J. L., "A Suggested Semi-Empirical Method for the Calculation of the Boundary Layer Transition Region," Dept. of Aerospace Engineering, Delft Univ. of Technology, Rept. VTH-74, Delft, The Netherlands, 1956.

[14] Smith, A. M. O., and Gamberoni, N., "Transition, Pressure Gradient, and Stability Theory," Douglas Aircraft Co., Rept. ES 26338, Long Beach, CA, 1956.

[15] *CFL3D Version 6* [online database], http://cfl3d.larc.nasa.gov/Cfl3dv6/cfl3dv6.html [retrieved 1 Nov. 2005].

[16] Roe, P. L., "Approximate Riemann Solvers, Parameter Vectors and Difference Schemes," *Journal of Computational Physics*, Vol. 43, 1981, pp. 357–372.
doi:10.1016/0021-9991(81)90128-5

[17] Menter, F. R., "Two-Equation Eddy-Viscosity Turbulence Models for Engineering Applications," *AIAA Journal*, Vol. 32, No. 8, 1994, pp. 1598–1605.

[18] Jones, W. P., and Launder, B. E., "The Prediction of Laminarization with a Two-Equation Model of Turbulence," *International Journal of Heat and Mass Transfer*, Vol. 15, 1972, pp. 301–314.
doi:10.1016/0017-9310(72)90076-2

[19] Spalart, P., and Allmaras, S., "A One-Equation Turbulence Model for Aerodynamic Flows," AIAA Paper 92-0439, 1992.

[20] Weiss, J. M., and Smith, W. A., "Preconditioning Applied to Variable and Constant Density Flows," *AIAA Journal*, Vol. 33, No. 11, 1995, pp. 2050–2057.

[21] Pauley, L. L., Moin, P., and Reynolds, W. C., "The Structure of Two-Dimensional Separation," *Journal of Fluid Mechanics*, Vol. 220, 1990, p. 397.
doi:10.1017/S0022112090003317

[22] McGhee, R. J., Walker, B., and Millard, B., "Experimental Results for the Eppler 387 Airfoil at Low Reynolds Numbers in the Langley Low-Turbulence Pressure Tunnel," NASA TM 4062, 1988.

[23] Liebeck, R. H., and Camacho, P. P., "Airfoil Design at Low Reynolds Number with Constrained Pitching Moment," Conference on Low Reynolds Number Airfoil Aerodynamics, Univ. of Notre Dame, Paper UNDAS CP-77B123, 1985.